IOPscience iopscience.iop.org

Home Search Collections Journals About Contact us My IOPscience

Mapping the excited-state bands above the vacuum level with VLEED: principles, results for Cu, and the connection to photoemission

This article has been downloaded from IOPscience. Please scroll down to see the full text article.

1996 J. Phys.: Condens. Matter 8 7539

(http://iopscience.iop.org/0953-8984/8/41/004)

View the table of contents for this issue, or go to the journal homepage for more

Download details:
IP Address: 171.66.16.207
The article was downloaded on 14/05/2010 at 04:16

Please note that terms and conditions apply.

J. Phys.: Condens. Matter **8** (1996) 7539–7547. Printed in the UK

Mapping the excited-state bands above the vacuum level with VLEED: principles, results for Cu, and the connection to photoemission

V N Strocov†, H I Starnberg‡§ and P O Nilsson‡

† International Institute of Interphase Interactions, PO Box 1146, 194291 St Petersburg, Russia
‡ Department of Physics, Chalmers University of Technology and Göteborg University, S-412 96 Göteborg, Sweden

Received 5 January 1996, in final form 9 May 1996

Abstract. Experimental photoelectron spectra are usually interpreted using rather crude approximations for the upper states into which the electrons are excited. Better knowledge about these excited states could substantially improve the accuracy of valence band mapping by photoelectron spectroscopy. We here demonstrate that VLEED measurements are ideally suited for accurate determination of the desired upper states. This is illustrated by model calculations including absorption and self-energy corrections. The close correspondence between so-called irregularity points of the excited-state bands and the total electron reflectivity is established, which opens up the possibility for direct mapping of irregularity points by comparison with experimental VLEED spectra, and for fitting of the whole excited-state bands between these points. The proposed scheme is finally used to determine the excited-state bands of Cu along ΓL from measurements on Cu(111).

1. Introduction

The photoemission process inherently employs a lower state (hole), and an upper state (electron). To obtain the dispersion of the lower bands perpendicular to the surface, one needs to know the dispersion of the corresponding upper ones. One approach here is using the upper bands as computed with a ground-state potential (those bands are further referred to as the *ground-state bands* $\varepsilon(\boldsymbol{k})$). However, the upper states essentially refer to an excited state of a solid [1, 2], and may significantly differ from the ground-state bands. An alternative approach is to neglect the scattering by the crystal potential and use free-electron bands instead, as the excited-state effects make the upper bands more free-electron-like. In general, both of these approaches are inadequate when high accuracy is essential.

Neglecting the electron–hole interactions, the upper states may be accurately described as independent excited-state electrons of finite lifetime τ, if all electron interactions are described by introducing an effective complex non-local potential. Due to the finite lifetime of the excited-state electrons, their energies are blurred. They are described by the spectral function $A(\boldsymbol{k}, \omega)$, which gives the probability of observing an electron of momentum $\boldsymbol{k}$ and energy $\hbar\omega$. Generally, $A(\boldsymbol{k}, \omega)$ is peaked at some energy E; the peak halfwidth is related to the lifetime as $\hbar/\tau$. The complex self-energy Σ combines these quantities: $\Sigma = E + \mathrm{i}\hbar/\tau$.

§ Author to whom any correspondence should be addressed.

0953-8984/96/417539+09$19.50 © 1996 IOP Publishing Ltd

The spectral function description is numerically very involved. An approximation is made [3, 4] by characterizing the excited-state electrons by wavefunctions $\varphi(\boldsymbol{r}, t)$, which decay exponentially in time: $\varphi(\boldsymbol{r}, t) \sim \varphi(\boldsymbol{r}) \exp[-\mathrm{i}Et/\overline{h}] \exp[-t/\tau]$, where E stands for $\mathrm{Re}\,\Sigma$, and $\overline{h}/\tau = \mathrm{Im}\,\Sigma$. These wavefunctions should satisfy the time-dependent Schrödinger equation $(\hat{\mathcal{H}}^{eff} - \mathrm{i}\overline{h}\,\partial/\partial t)\varphi(\boldsymbol{r}, t) = 0$, where $\hat{\mathcal{H}}^{eff}$ includes the effective non-local Hermitian potential V^{eff} describing the electron interactions. This equation then reduces to an equation for the time-independent part $\varphi(\boldsymbol{r})$ only:

$$(\hat{\mathcal{H}}^{eff} - E + \mathrm{i}\overline{h}/\tau)\varphi(\boldsymbol{r}) = 0.$$

Introducing the so-called imaginary (absorption) potential V_i as $V_i = \overline{h}/\tau$, we arrive at

$$(\hat{\mathcal{H}}^{eff} - E + \mathrm{i}V_i)\varphi(\boldsymbol{r}) = 0.$$

This looks exactly like a stationary Schrödinger equation, except that the stationary energy is replaced by the complex energy $E - \mathrm{i}V_i$, or the complex conjugate of the self-energy Σ.

To find the excited states in a crystal, one solves the above equation with a periodic V^{eff}. Its solutions $\varphi(\boldsymbol{r})$ are damped Bloch waves, whose wavevector $\boldsymbol{k}$ is complex with the imaginary part $\mathrm{Im}\,\boldsymbol{k}$ causing $\varphi(\boldsymbol{r})$ to decay. Therefore, an excited state in a crystal is characterized by a complex self-energy Σ depending on a complex wavevector $\boldsymbol{k}$. Bands of the real part of Σ, depending on complex $\boldsymbol{k}$, are referred to as the *excited-state bands* $E(\boldsymbol{k})$.

The excited-state bands $E(\boldsymbol{k})$ are shifted from the ground-state bands $\varepsilon(\boldsymbol{k})$. The difference is referred to as the self-energy correction $\Sigma'(\boldsymbol{k}, \varepsilon)$. One can distinguish two contributions to the self-energy correction $\Sigma'(\boldsymbol{k}, \varepsilon)$. The first contribution is due to the imaginary absorption potential V_i, which acts to smooth the bands near the band gaps. The second one is due to the significant difference of the excited-state V^{eff} (depending on $\boldsymbol{r}$, E and $\boldsymbol{k}$), from the ground-state crystal potential $V(\boldsymbol{r})$. This contribution produces systematic energy shifts of the bands. In the following we refer to the bands calculated with V^{eff}, but without absorption V_i, as no-absorption bands. (In fact, most available so-called quasiparticle calculations produce essentially the no-absorption bands [5].)

When calculating the excited-state upper bands of photoemission, it is usually not difficult to assess V_i properly. However, theoretically very little is known exactly about the excited-state V^{eff}, which has to incorporate all electron interactions, and which produces significant self-energy corrections. In order to obtain a proper description of the upper bands, these self-energy corrections have to be determined experimentally.

The most direct experimental probe for bands above the vacuum level is the very-low-energy electron diffraction (VLEED) technique [6, 7], reviewed in [8]. A particular advantage of VLEED is that only one electronic state is involved. The relevance of VLEED to photoemission is established from the one-step photoemission theory [9, 10, 11]. Neglecting the electron–hole interaction, the photocurrent $I_\nu(E)$ from the νth initial state Φ_ν is given by

$$I_\nu(E) \propto |\langle \Phi^{L*} | \boldsymbol{A} \cdot \boldsymbol{p} | \Phi_\nu \rangle|^2$$

where $\boldsymbol{A}$ is the screened vector potential of the electric field, $\boldsymbol{p}$ is the momentum operator, and Φ^L is exactly the LEED wavefunction, which would be excited in the crystal by incident electrons coming from the photoemission detector.

The theoretical foundation for VLEED investigations is the matching approach [12, 13, 14], which links the elastic reflectivity $R(E)$ to the properties of the Bloch waves excited in a crystal, including their dispersion. However, detailed band mapping from VLEED data was demonstrated only recently [15, 16, 17], using the no-absorption approximation. It has been found that an incident beam of energy E and parallel wave-vector component

$\boldsymbol{K}_\parallel$ significantly excites only so-called *coupling bands*. These bands are defined as those, among all bands available for given E and $\boldsymbol{K}_\parallel$, having the maximal amplitude of the Fourier component similar to the incident plane wave (the so-called conducting component). The behaviour of $R(E)$ is mainly determined by the features of the coupling bands. In contrast, bands with negligible amplitude of the conducting component (so-called *non-coupling* bands) are not excited by the incident beam, and do not influence $R(E)$. In the vicinity of the *critical points* (CPs) (defined as the points where the slope of the bands $\mathrm{d}E/\mathrm{d}k_\perp$ undergoes sharp changes, or vanishes at the band-gap edges) of the coupling bands, the rapid changes in wave-function composition also give rise to rapid changes of $R(E)$, through the matching on the surface. Therefore, each CP of the coupling bands produces an extremum in the derived spectrum $\mathrm{d}R/\mathrm{d}E$. By comparing the positions of experimental and calculated extrema of $\mathrm{d}R/\mathrm{d}E$, the empirical positions of relevant CPs were found. Moreover, whole bands in symmetry planes of the Brillouin zone (BZ) were mapped from the dispersion of CPs situated there, upon variation of $\boldsymbol{K}_\parallel$.

It may seem straightforward to proceed to the excited-state description by replacing the no-absorption bands by the complex excited-state bands, represented by $E(\mathrm{Re}\,\boldsymbol{k})$. However, in contrast to the sharp no-absorption bands, the excited-state bands are rather featureless, due to the effect of the absorption potential V_i. This has prevented us from establishing their correlation with $R(E)$.

In this paper we apply model calculations to illustrate that, despite the featureless appearance of excited-state bands, one can uncover well-defined irregularity points (IPs) in them, which are linked to the extrema of $\mathrm{d}R/\mathrm{d}E$ in the same way as the CPs of no-absorption bands. Consequently, the experimental positions of IPs can be determined from VLEED data. Moreover, by fitting a reference calculation to the experimental IPs, empirical excited-state bands are obtained as a whole.

2. Model calculations

Our model calculations consider normal incidence of an electron beam onto the (100) surface of a hypothetical cubic crystal. The reflectivity $R(E)$ is directly related to the band structure along $\Gamma\mathrm{X}$, through the conservation of parallel momentum ($\boldsymbol{k}_\parallel = 0$). The model includes general band-structure features, and is analogous to normal incidence onto the (111) surface of any typical fcc metal (like, e.g., Cu, Ni, or Al) [6].

The excited-state effects were described with a local pseudopotential $V^{ps}(\boldsymbol{r})$ approximating the excited-state potential V^{eff}, and the absorption potential $\mathrm{i}V_i$. The excited-state bands (E as functions of the complex $\boldsymbol{k}$, with $\boldsymbol{k}_\parallel = 0$) were found by solving the secular equation with respect to $\boldsymbol{k}$:

$$\det[(|\boldsymbol{k}+\boldsymbol{G}|^2 - E + \mathrm{i}V_i)\delta_{\boldsymbol{G}-\boldsymbol{G}'} + V^{ps}_{\boldsymbol{G}-\boldsymbol{G}'}] = 0$$

where $V^{ps}_{\boldsymbol{G}-\boldsymbol{G}'}$ are the pseudopotential matrix elements connecting the symmetrized plane waves corresponding to $\boldsymbol{G}$ and $\boldsymbol{G}'$. E stands for $\mathrm{Re}\,\Sigma$, comprising the ground-state energy and the self-energy corrections. The wave vectors are measured in units of $2|\Gamma\mathrm{X}|$, and the energies in units of $(2|\Gamma\mathrm{X}|)^2$. Through the symmetry of the model, the basis set was reduced to six symmetrized plane waves of Δ_1 symmetry, corresponding to the six non-equivalent lowest-energy bulk reciprocal vectors $\boldsymbol{G}$. By virtue of the local V^{ps}, the secular equation was reduced to an eigenvalue problem, with complex $\boldsymbol{k}$-values appearing as the eigenvalues of a complex double-dimensioned matrix, constructed from the Hamiltonian matrix [13, 18].

The reflectivity $R(E)$ was calculated by the matching approach [12, 13, 14], assuming a step-like surface barrier. The vacuum wavefunction is the sum of the incident plane wave,

and all diffracted ones, each corresponding to a surface reciprocal vector $\boldsymbol{g}$:

$$\Phi_v = \exp[\mathrm{i}\boldsymbol{K}\cdot\boldsymbol{r}] + \sum_g R_g \exp[-\mathrm{i}\boldsymbol{K}^g\cdot\boldsymbol{r}].$$

The wavefunction excited in the crystal is a linear combination of all available decaying Bloch waves ϕ_n, for given E and $\boldsymbol{K}_\parallel$:

$$\Phi_c = \sum_n T_n\phi_n.$$

Φ_v and Φ_c were expanded over the symmetrized combinations of the surface-parallel plane waves $\exp[\mathrm{i}(\boldsymbol{k}_\parallel + \boldsymbol{g})\cdot\boldsymbol{r}]$, corresponding to the two shortest non-equivalent $\boldsymbol{g}$, and the unknown amplitudes R_g and T_n were found by component-by-component matching of Φ_v and Φ_c in a plane placed at half an interatomic distance from the topmost atomic layer. The total reflectivity $R(E)$ was found by summation over all diffracted beams:

$$R(E) = \sum_g |R_g|^2 \,\mathrm{Re}\, K_\perp^g/K.$$

3. Correlation of excited-state bands with $R(E)$

We have performed model calculations for various pseudopotentials V^{ps} and absorption potentials V_i. Figure 1 displays the results, obtained with realistic values of $V^{ps}_{G-G'}$ (1–1.5 eV).

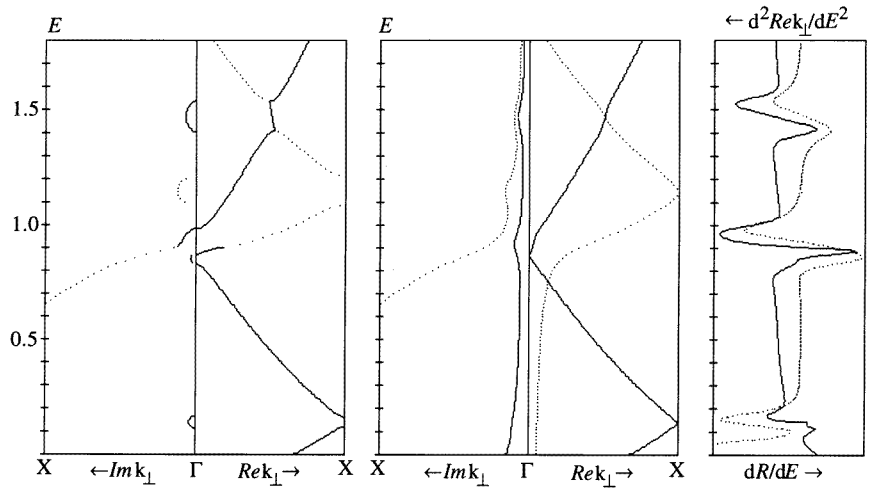

Figure 1. Model calculations on a cubic-lattice crystal, corresponding to normal incidence onto the (100) surface. Left: the no-absorption bands, calculated with vanishing V_i. Centre: the excited-state bands calculated with $V_i = 0.05$, which resembles the absorption for typical fcc metals; the bands coupling to the incident plane wave are shown by solid lines. Right: the IPs of excited-state coupling bands visualized as the extremes of a plot of $\mathrm{d}^2\,\mathrm{Re}\,k_\perp/\mathrm{d}E^2$ (the solid line), and manifested in electron reflection as the extremes of a plot of $\mathrm{d}R/\mathrm{d}E$ (the dotted line). Energy is measured in units of $(2|\Gamma\mathrm{X}|)^2$; $\mathrm{d}^2\,\mathrm{Re}\,k_\perp/\mathrm{d}E^2$ and $\mathrm{d}R/\mathrm{d}E$ are measured in arbitrary units. The principal pseudopotential Fourier components V_{100}, V_{110}, V_{200}, V_{210} are set to 0.03, V_{000} to -0.1, and the rest to zero.

With negligible absorption V_i (figure 1, left), the no-absorption bands are basically the ground-state ones (apart from a systematic energetic shift, as we have assumed V^{ps} corresponding to the excited state V^{eff}). However, due to the presence of the surface, damped Bloch waves with complex $k_\perp$ are allowed [4, 18, 19], in addition to the propagating ones with real $k_\perp$. This results in the 'real lines' linking bands with real $k_\perp$ across their gaps in plots of $E(\mathrm{Re}\, k_\perp)$.

Among all of the bands available for given E and $\boldsymbol{K}_\parallel$, the incident beam predominantly excites the coupling bands, defined in previous papers as the bands having the maximal amplitude of the conducting Fourier component, which is associated with the incident plane wave through $\boldsymbol{k}_\parallel + \boldsymbol{G}_\parallel = \boldsymbol{K}_\parallel$ [7, 16]. In the light of explicit matching calculations this definition may be refined as follows: the coupling bands are the bands which, for given E and $\boldsymbol{K}_\parallel$, have the maximal excitation (transmission) amplitude $|T_n|$, provided that the Bloch waves are all normalized as

$$\int \phi_n^*(\boldsymbol{r})\phi_n(\boldsymbol{r})\ \mathrm{d}\boldsymbol{r} = 1$$

where the integration is over the crystal half-space. Thereby, the coupling bands are associated with the maximum of partial probability

$$|T_n|^2 \int \phi_n^*(\boldsymbol{r})\phi_n(\boldsymbol{r})\ \mathrm{d}\boldsymbol{r}$$

of an electron being in the crystal. (This is not equivalent to the maximum of the Bloch wave amplitude $|T_n||\phi_n(\boldsymbol{r})|$ on the surface. Physically, our definition accounts for the fact that a strongly damped Bloch wave contributes less to the total electron transmission.) The coupling bands are shown in figure 1 as solid lines. Usually they are associated with the minimal $\mathrm{Im}\, k_\perp$. The other bands shown may be characterized as non-coupling bands if they are well beyond the regions of hybridization with the coupling bands, because there they lose the conducting Fourier component, and their T_n vanish. Bands characterized by not totally symmetric wave functions have been excluded in the calculation. They are classified as non-coupling bands as well, because their excitation amplitude $T_n = 0$ due to their lack of any conducting component.

The critical points (CPs) of bands corresponding to propagating Bloch waves were previously determined either from sharp variations, or vanishing, of their slope $\mathrm{d}E/\mathrm{d}k_\perp$. However, with the damped Bloch waves $\mathrm{d}E/\mathrm{d}\,\mathrm{Re}\, k_\perp$ goes to infinity along the vertical real lines. The bands are therefore more conveniently characterized by their inverse slope $\mathrm{d}\,\mathrm{Re}\, k_\perp/\mathrm{d}E$. Generalizing previous definition, the CPs are redefined as the points with either sharp variations, or singularities, of the inverse slope $\mathrm{d}\,\mathrm{Re}\, k_\perp/\mathrm{d}E$.

By including absorption $\mathrm{i}V_i$, one obtains realistic excited-state bands. Figure 1, centre, shows the bands calculated with $V_i = 0.05$ (for typical fcc metals this value corresponds to approximately 1.7 eV, which is reasonable up to 30 eV relative to E_{vac}). The coupling bands are again shown as solid lines. In comparison with the no-absorption bands, the excited-state bands look rather smooth.

However, one may notice that each CP has become a point with a perceptible irregularity of the excited-state band, in which the band still distinctly changes its slope $\mathrm{d}\,\mathrm{Re}\, k_\perp/\mathrm{d}E$. To distinguish these points from the sharp no-absorption CPs, we classify these points as irregularity points (IPs). They are readily revealed as the extremal points of the plot $\mathrm{d}^2\,\mathrm{Re}\, k_\perp/\mathrm{d}E^2$ (figure 1, right, full line, displayed for the coupling band only), which may be interpreted as corresponding to the perpendicular effective mass $m^* \sim \mathrm{d}^2k_\perp/\mathrm{d}E^2$ of the propagating states. (In the no-absorption limit, $\mathrm{d}^2\,\mathrm{Re}\, k_\perp/\mathrm{d}E^2$ may exhibit singularities at CPs.)

Generally, the wavefunction composition undergoes drastic changes whenever a band passes through an IP. If an IP belongs to the coupling bands, the matching on the surface results in a sharp change of $R(E)$, or an extremum of the curve of $\mathrm{d}R/\mathrm{d}E$ (figure 1, right, dotted line). The energy difference between an IP and the corresponding extremum of $\mathrm{d}R/\mathrm{d}E$ hardly exceeds 5% of the band width, so as a rule each extremum of $\mathrm{d}R/\mathrm{d}E$ can be uniquely assigned to an IP.

Our calculations reveal some further aspects of the relationship between excited-state bands and electron reflectivity.

(i) The correspondence between IPs and extrema of $\mathrm{d}R/\mathrm{d}E$ is rather insensitive to the position and shape of the surface barrier. For example, variation of the matching plane position by a quarter of the interlayer distance shifted the energetic positions by less than 0.015.

(ii) The non-coupling bands, which are not excited by the incident wave, do not produce any structure in $\mathrm{d}R/\mathrm{d}E$. An example is the 'invisible' irregularity at the BZ border near $E = 1.15$ (figure 1).

(iii) Often a multitude of bands exist for given E and $\boldsymbol{K}_{\parallel}$, particularly for off-symmetry incidence. In such cases visual inspection of the bands is not sufficient for identifying the coupling bands. Instead they can be identified by evaluation of the Bloch-wave excitation amplitudes T_n during a reference calculation with an approximate potential.

(iv) If several IPs are close in energy, as compared to the absorption value V_i, the corresponding features of $\mathrm{d}R/\mathrm{d}E$ may overlap. Such overlap may hide the one-to-one correspondence of IPs and extrema of $\mathrm{d}R/\mathrm{d}E$. For example, the two minor irregularities recognized as a shoulder of $\mathrm{d}^2 \operatorname{Re} k_\perp/\mathrm{d}E^2$ near $E = 0.8$ are hardly distinguished in $\mathrm{d}R/\mathrm{d}E$.

(v) The IPs of the coupling bands are linked to the total reflectivity $R(E)$, rather than to the specular reflectivity. For example, at the two IPs near $E = 1.5$ the reflectivity is redistributed to non-specular beams of the type $\exp[-\mathrm{i}(\boldsymbol{K} + \boldsymbol{g}_{10}) \cdot \boldsymbol{r}]$, while the specular reflection vanishes. This fact strongly favours use of the target current spectroscopy (TCS) experimental technique [16, 20], which measures the total reflectivity $R(E)$ by recording the current absorbed by the sample.

(vi) When switching on the absorption, CPs of the no-absorption bands generally transform to become IPs of the excited-state bands, without substantial energy shifts. Therefore, the extrema of $\mathrm{d}R/\mathrm{d}E$ may also be thought of as manifesting CPs of no-absorption bands. This fact justifies the previously applied method of no-absorption band mapping.

(vii) Also the curves of $E(\operatorname{Im} k_\perp)$ are related to $R(E)$, in that any loop-like bump of $E(\operatorname{Im} k_\perp)$, related to a coupling band, is associated with a reflectivity peak.

4. Experimental excited-state band mapping by VLEED: mapping of IPs, band mapping, and band fitting

We have shown that the IPs of the coupling excited-state bands are associated with adjacent extrema of $\mathrm{d}R/\mathrm{d}E$. However, prior to the mapping one has to perform a reference calculation with an approximate crystal potential in order to establish this association unambiguously.

Mapping of IPs is particularly simple when they are well separated, so that their one-to-one correspondence with extrema of $\mathrm{d}R/\mathrm{d}E$ is upheld. The experimental energy of any IP is then obtained by correcting its calculated position with the energy shift of the corresponding experimental extremum of $\mathrm{d}R/\mathrm{d}E$ relative to its calculated counterpart. When a multitude

of closely spaced IPs results in overlapping extrema of $\mathrm{d}R/\mathrm{d}E$, one can still map the IPs by iterating the potential parameters of the reference calculation until the calculated extrema of $\mathrm{d}R/\mathrm{d}E$ fit their experimental energies. This kind of numerical fitting offers better accuracy than a simple empirical correction.

Continuous bands in the symmetry planes of the BZ may, in principle, be determined by a *band-mapping* procedure. For example, near $E = 0.15$ (figure 1, right) the band intersection with the BZ border may be located as the half-way point between the corresponding IPs. By mapping these points with respect to incidence $K_{\|}$, one obtains the corresponding band in the BZ symmetry planes. However, these bands are less applicable in photoemission due to their insignificant coupling at the relevant surface.

To obtain continuous coupling bands for further applications, *band fitting* to the experimental IPs is applied. The simplest method is to apply to the reference bands an energy-dependent shift, which varies linearly between the available energy shifts of the experimental IPs. Better accuracy is achieved by iterating the potential parameters of a reference calculation until the calculated extrema of $\mathrm{d}R/\mathrm{d}E$ fit their experimental energies. By this procedure, the IPs appear in their experimental positions simultaneously with the entire coupling bands connecting them. The non-coupling bands are not accurately located with the above procedure, as they have little influence on $R(E)$. However, these bands are not of much interest for practical applications.

5. Prospects for photoemission applications

The crucial point for the applications of VLEED in photoemission is that the final state of photoemission Φ^{L*} is exactly a time-reversed LEED wavefunction. In VLEED, the coupling bands were defined as those effectively matching the incident plane wave. In the time-reversed photoemission process, exactly the same coupling bands effectively match the outgoing plane wave, predominantly contributing to the photocurrent [21]. This means that the outlined empirical procedure for band fitting by VLEED provides exactly the dominant, or coupling, upper bands of photoemission.

The bands generated in this way have three attractive advantages for photoemission. Firstly, they account for the electron scattering by the crystal potential. Secondly, they account for the smoothing of excited-state bands due to finite lifetime. Thirdly, they include the experimental points measured by VLEED, to absorb the self-energy corrections due to the excited-state crystal potential V^{eff}. Even if the upper bands are close to an empirical free-electron parabola $E = |\boldsymbol{k} + \boldsymbol{G}|^2 + V_{000}$, the experimental points provided by VLEED resolve any ambiguities in the choice of the inner potential V_{000}.

Applying the above excited-state bands, one should be aware that the energetic positions of photoemission peaks may be somewhat displaced from the positions dictated by $k_{\perp}$-conservation. This may happen if the matrix element of the electric field, or the surface transmission factor, undergo sharp changes across the $k_{\perp}$-conserving Lorentzian [9, 22, 23]. This effect is expected to be notable near the IPs.

6. Example: excited-state band fitting for Cu along ΓL

The band fitting discussed above was applied to Cu to generate the excited-state bands along ΓL. The experimental VLEED spectra were obtained from the Cu(111) surface using the TCS technique [15]. The calculations along ΓL were made by the empirical pseudopotential method, employing a basis set of 7 symmetrized plane waves. A non-symmetry calculation

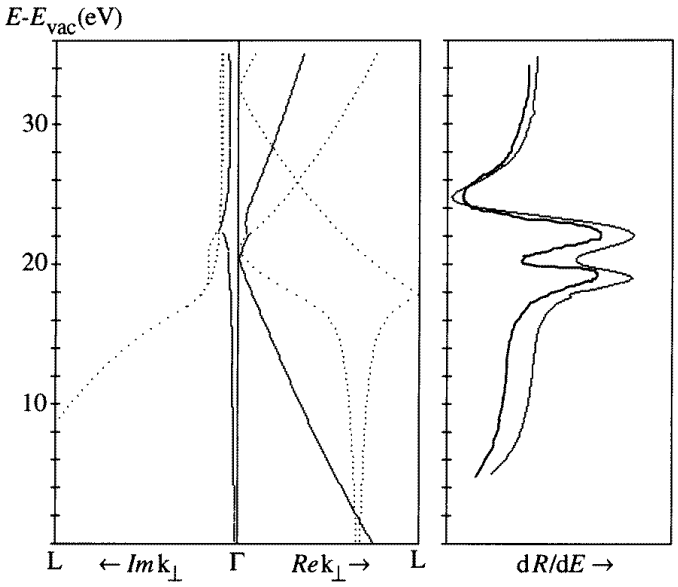

Figure 2. Normal incidence onto the Cu(111) surface. Left: the excited-state bands along ΓL generated with the optimized pseudopotential ($V_{200} = 0.4$ eV, $V_{220} = -0.7$ eV, $V_{222} = -1.6$ eV, $V_{000} = -13.4$ eV); the coupling bands are shown as solid lines. Right: calculated, and experimental (the bold line) $\mathrm{d}R/\mathrm{d}E$. The energies of their extrema match each other within the RMS error 0.18 eV.

employed 15 plane waves. The absorption was taken as $V_i = 0.05(E - E_F)$, as determined by photoemission measurements [1]. A step-like surface barrier was placed half an interlayer distance from the topmost atomic layer.

Figure 2, left, shows the excited-state bands generated with the optimized pseudopotential. The coupling bands are fairly well described by three Fourier components V_{200}, V_{220}, V_{222}, and the inner potential V_{000}. Despite the substantial absorption ($V_i \approx 1.3$ eV) they feature four closely spaced IPs near Γ. In $\mathrm{d}R/\mathrm{d}E$ (figure 2, right), these IPs produce a rather complicated superposition of overlapping features. Fitting the experimental data there turned out to be an ill-posed problem in the sense that there were a number of regions in V_{hkl}-space, each producing a calculated spectrum of $\mathrm{d}R/\mathrm{d}E$ compatible with the experimental data, but somewhat different bands. However, a constraint $|V_{220} + V_{222}| = 1.3$ eV was found from the particular band gap at $K_\parallel = 0.5|\Gamma\mathrm{X}|$ in the $\bar{\Gamma}\bar{\mathrm{K}}$ azimuth, by fitting the relevant off-symmetry experimental spectrum [15]. The constraint determined the unique region in V_{hkl}-space where the fit was further improved by varying the Fourier components independently. This allowed us to correct for the dependence of the pseudopotential on $\boldsymbol{k}$.

Near Γ, the experimental bands along ΓL deviate significantly from the free-electron bands. The difference motivates corrections of $k_\perp$ by up to 6% of $|\Gamma\mathrm{L}|$, which is substantial enough in accurate photoemission band mapping of the occupied states. While the lower d bands are too flat near Γ to be seriously affected, we expect corrections to the lowest p-band dispersion of almost 0.25 eV. Reconsidering the available photoemission data [24], it appears that the corrected $k_\perp$ improves somewhat the agreement with the calculated p band at higher photon energies, but more accurate photoemission measurements are required there.

7. Conclusion

A realistic description of the upper bands of photoemission should involve the excited-state bands, characterized by a complex self-energy Σ depending on a complex wavevector $\boldsymbol{k}$. Accurate calculations are not yet feasible, but one can derive them experimentally using VLEED.

The principles of VLEED band mapping were derived using a model calculation. Despite being smooth, the excited-state bands are characterized by well-defined irregularity points (IPs), where the inverse slope of the plots of Re Σ (Re $k_\perp$) undergoes sharp variations. The IPs are closely related to the critical points (CPs) of the no-absorption bands. Each IP produces an extremum in $\mathrm{d}R/\mathrm{d}E$ if the corresponding band couples to the incident plane wave. This allows experimental mapping of IPs by comparison with experimental spectra. Moreover, the coupling bands as a whole may be determined between the experimental IPs by a band-fitting procedure, when one fits the experimental position of extrema of $\mathrm{d}R/\mathrm{d}E$ by iterating the crystal potential involved in calculations. These bands, which include the experimental self-energy corrections, are straightforward for use as upper states in photoemission.

We have performed excited-state band fitting for Cu along the ΓL line, using experimental VLEED data for the Cu(111) surface. Near Γ the excited-state bands maintained a significant difference from the free-electron bands. These effects are far more prominent for non-metals, due to stronger scattering potentials [11, 25].

References

[1] Goldmann A, Altmann W and Dose V 1991 *Solid State Commun.* **79** 511
[2] Nilsson P-O, Kanski J and Larsson C G 1980 *Solid State Commun.* **36** 111
[3] Pendry J B 1974 *Low Energy Electron Diffraction* (London: Academic)
[4] Dederichs P H 1972 *Solid State Physics* vol 27, ed H Ehrenreich, F Seitz and D Turnbull (New York: Academic) p 136
[5] Jenkins S J, Srivastava G P and Inkson J C 1993 *Phys. Rev.* B **48** 4388
[6] Jaklevic R C and Davis L C 1982 *Phys. Rev.* B **26** 5391
[7] Strocov V N 1991 *Solid State Commun.* **78** 845
[8] Strocov V N 1995 *Int. J. Mod. Phys.* B **9** 1755
[9] Feibelman P J and Eastman D E 1974 *Phys. Rev.* B **10** 4932
[10] Pendry J B 1976 *Surf. Sci.* **57** 679
[11] Pehlke E and Schattke W 1987 *J. Phys. C: Solid State Phys.* **20** 4437
[12] Capart G 1969 *Surf. Sci.* **13** 361
[13] Pendry J B 1969 *J. Phys. C: Solid State Phys.* **2** 2273
[14] Jepsen D W, Marcus P M and Jona F 1972 *Phys. Rev.* B **5** 3933
[15] Strocov V N and Komolov S A 1991 *Phys. Status Solidi* b **167** 605
[16] Strocov V N 1993 *Int. J. Mod. Phys.* B **7** 2813
[17] Strocov V N and Starnberg H I 1995 *Phys. Rev.* B **52** 8759
[18] Smith D L and Mailhiot C 1990 *Rev. Mod. Phys.* **62** 173
[19] Stampfl C, Kambe K, Riley J D and Lynch D F 1992 *J. Phys.: Condens. Matter* **2** 8461
[20] Komolov S A 1992 *Total Current Spectroscopy of Surfaces* (Philadelphia, PA: Gordon and Breach)
[21] Mahan G D 1970 *Phys. Rev.* B **2** 4334
[22] Pehlke E and Schattke W 1989 *Solid State Commun.* **69** 419
[23] Jepsen D W, Himpsel F J and Eastman D E 1982 *Phys. Rev.* B **26** 4039
[24] Petroff Y and Thiry P 1980 *Appl. Opt.* **19** 3957
[25] Olde J, Mante G, Barnscheidt H-P, Kipp L, Kuhr J-C, Manzke R, Skibowski M, Henk J and Schattke W 1990 *Phys. Rev.* B **41** 9958